
Article:
Kennedy, C.R., Jaksic, V., Leen, S.B. et al. (2018) Fatigue life of pitch- and stall-regulated composite tidal turbine blades. Renewable Energy, 121. pp. 688-699. ISSN: 0960-1481

https://doi.org/10.1016/j.renene.2018.01.085

Fatigue life of pitch- and stall-regulated composite tidal turbine blades

Ciaran R. Kennedy[1], Vesna Jaksic[2*], Sean B. Leen[1] and Conchúr M. Ó Brádaigh[3]

[1]Mechanical Engineering, NUI Galway, Ireland

[2]Sustainable Infrastructure Research & Innovation Group (SIRIG), Civil, Structural and Environmental Engineering Department, Cork Institute of Technology, Ireland

[3]School of Engineering, Institute for Materials and Processes, University of Edinburgh, Scotland, UK

*Corresponding Author: Vesna Jaksic (vesna.jaksic@cit.ie)

Summary: Tidal turbine blades are subject to harsh loading and environmental conditions, including large thrust and torsional loadings, relative to wind turbine blades, due to the high density of seawater, among other factors. The complex combination of these loadings, as well as water ingress and associated composite laminate saturation, have significant implications for blade design, affecting overall device design, stability, scalability, energy production and cost-effectiveness. This study investigates the effect of seawater ingress on composite material properties, and the associated design and life expectancy of tidal turbine blades in operating conditions. The fatigue properties of dry and water-saturated glass fibre reinforced laminates are experimentally evaluated and incorporated into tidal blade design. The fatigue lives of pitch- and stall-regulated tidal turbine blades are found to be altered by seawater immersion. Water-saturation is shown to reduce blade life about 3 years for stall-regulated blades and by about 1 to 2 years for pitch-regulated blades. The effect of water ingress can be compensated by increased laminate thickness. The tidal turbine blade design methodology presented here can be used for evaluation of blade life expectancy and tidal device energy production.

Keywords: Tidal energy, tidal blade design, stall-regulated HATT, and pitch-regulated HATT, composite materials, fatigue life.

Corresponding Author: Vesna Jaksic, Lecturer, Civil, Structural and Environmental Engineering Department, Cork Institute of Technology, Cork, Ireland.

Phone: 00353-(0)21-432-6762. Email: vesna.jaksic@cit.ie

---

1. Introduction

Tidal energy is is gaining increased importance as a renewable energy source due to its high predictability over long timescales [1]. However, the tidal force can vary over a small geographical space [2], posing a challenge to the reliable long-term design of cost effective structures. The tidal force can vary locally within distances of tens of meters to tens of kilometres, due to the local bathymetry and seabed conditions. Hence, blade design requires particular attention. Current tidal turbine (TT) blade designs are largely based on wind turbine (WT) blade technology. But increasing appreciation of the specific and unique challenges of the tidal blade environment is leading to specific design evolution for tidal blades [3]. Tidal blades have to withstand the significant forces of seawater and turbulence flows, and must withstand water ingress and saturation during the device employment period [4, 5]. The most highly-developed TT technology is the horizontal axis tidal turbine (HATT), which converts the kinetic energy within the tidal stream into mechanical energy, via the hydrodynamic forces acting perpendicular to the rotor plane creating blade lift and rotation [5]. In order to stay within generator capacity, i.e. limit peak power, blade pitching can be used [6, 7]. However, blade failures on a number of prototypes emphasise the need for a design that will withstand the significant hydrodynamic loads during expected turbine life.

Composite materials, especially glass fibre reinforced polymers (GFRP), are the most commonly used materials for TT blade design due to their favourable characteristics, e.g. high specific strength and stiffness, resistance to corrosion and reasonable cost [5, 8]. The importance of environmental effects on the properties of composite materials has previously been recognised and studied [9, 10]. The specific application of composites in structural design of ocean energy structures has triggered studies on immersed performance of composites in seawater [11-13]. Studies show that immersed GFRP becomes moisture-saturated relatively early in its life. Hence, for TT blade design, it is important to understand durability and performance of these materials over the device lifetime.

The polymers normally used in GFRP can absorb up to 5% water by weight when immersed for long periods, changing the mechanical properties (e.g. reducing static tensile strength of the material by more than 25%) [14]. Water diffuses into the polymer matrix [13] and the multidirectional nature of laminates complicates the fatigue damage mechanisms. Matrix cracking parallel to the fibres or inter fibre failure (IFF) is first seen in the most off-axis plies under tensile fatigue loading. Most of the IFF cracking takes place in the first 25% of fatigue life and the significant drop in laminate stiffness is complete at this stage, with only a minor reduction in stiffness after this point. However, fatigue strength reductions do not follow the changes in static strength since the damage mechanisms are different in fatigue [15]. There is little test data available on material behaviour under coupled environmental and cycling loading [4]. An extensive review of fatigue modelling in GFRP has divided the work among three broad approaches [16]. First is a testing approach, where life predictions are based on test data of the exact or a similar material; second is a phenomenological approach, where predictions are based on the stiffness and residual strength behaviour; third, a progressive damage approach where damage in

the unidirectional (UD) lamina is predicted and incremented until a final failure state is reached, thereby predicting fatigue life. The testing approach to fatigue life estimation is the most widely used [17]. The technique is under continual evolution and refinement to include effects like spectral loading and complex constant life diagram (CLD) results [18]. Strength degrades continuously during fatigue and an early characterization model proposed that it degrades linearly per cycle, in constant amplitude fatigue [19, 20]. Key problems with all residual strength methods are the large scatter in the residual strength test results and the complexity of the degradation. The stiffness of GFRP laminates degrades by between 10 to 20% during fatigue cycling. The technique has been used to predict the life of particular WT blade laminates.

The main drawback of the latter models is a lack of flexibility in dealing with different laminate layups and/or loading patterns. Micromechanical approaches that predict the response of the laminate based on damage mechanisms in the individual UD plies offer a potential solution. The simplest approach is to degrade the matrix properties based on observed levels of cracking [21] and use classical laminate theory (CLT) to integrate the results. Others have considered two damage mechanisms, namely matrix cracking and interlaminar delamination [22]. Fracture mechanics approaches have been presented to predict matrix cracking behaviour and fibre failure; energy approaches have been used to model delamination, with stochastic methods used to enhance existing techniques. However, significant ongoing work is focussed on improving the capability for predicting test results and to reduce the amount of testing required to produce reliable fatigue life estimates. In order to fully utilise the TT blade structural material fatigue life, it is necessary to have information on its performance in the marine environment for the full design life of marine renewable energy devices (up to 20 years or so). The literature on fatigue test programs on the use of composite materials in marine renewable energy devices is, however, limited. Consequently, TT device design tends to be conservative, leading to cost penalties. A comprehensive fatigue life model for composite blades, incorporating realistic hydrodynamic loadings, cyclically-varying blade stresses and wet composite material fatigue properties would, therefore, be valuable tool for TT design.

The proposed TT blade fatigue design methodology consists of five modules [23] (Figure 1). The first module is a tidal model, which predicts the tidal current speed for relevant local tidal velocities measured [5, 23]. The output from this tidal model forms an input to a hydrodynamic model, which defines an aerofoil geometry (optimum chord length and pitch angle) and blade loadings (axial and tangential blade forces). The third module is a structural model. Based on the hydrodynamic module output, a finite element model of the blade is developed and factored forces are applied in order to determine the strain distribution in the turbine blade. The fatigue model determines the maximum strain in the blade for each rotation cycle. The maximum strains are compared to an experimentally-determined strain-life curve for the material and a damage fraction for that cycle is obtained. Summation of the damage fractions using Miner's rule gives an estimate for the life of the TT blade (TTB) [24]. In

this paper, we adopt this design approach in the context of the water ingression effect on the performance of stall- and pitch-regulated tidal turbine, in order to integrate fatigue life expectancy of water-immersed composites into blade design.

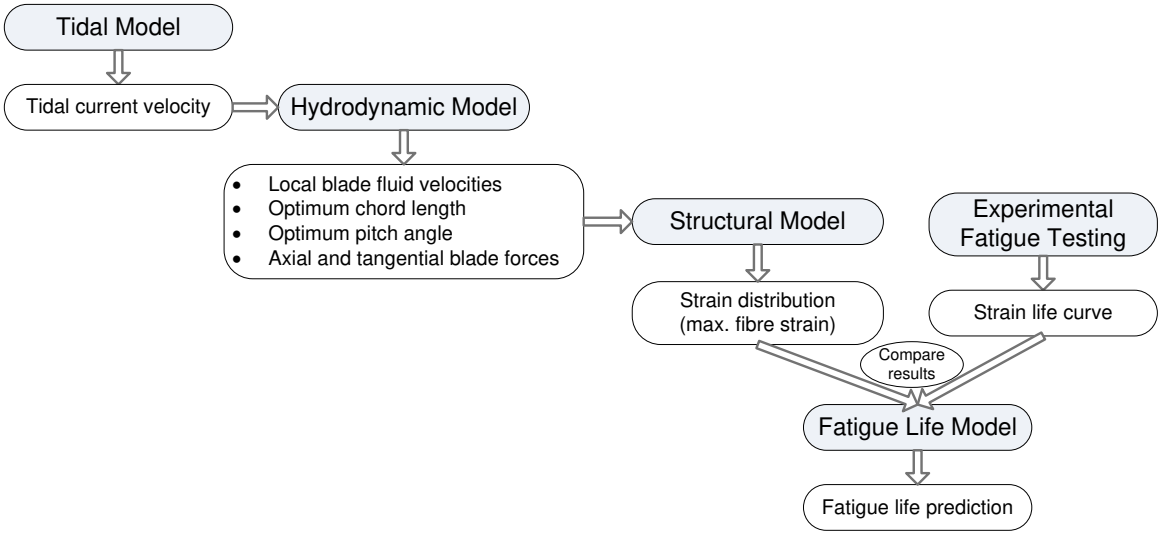

Figure 1. Tidal turbine blade design process algorithm.

2. Design Methodology

2.1 Tidal model

It is assumed here that the tidal phenomenon occurs twice within each period of 24 hours, 50 minutes and 28 seconds, consisting of two high and two low tides [25]. The highest tides, spring tides, occur when the sun and the moon line up with the earth. The lowest tides, neap tides, occur when the sun and moon are at 90° to each other. The current speed depends on the local topography. However, if the spring and neap maximum velocities are measured, the full cycle can be approximated by combining a semi-diurnal sinusoid and a fortnightly sinusoidal function [26]. The tidal current velocity, V_t, is:

$$V_t = cos(\omega_d t)[v_{ave} + v_{alt}\, cos(\omega_m t)] \quad (1)$$

where v_{ave} is the average of the peak tidal velocities, v_{alt} is half the range of peak tidal velocities, ω_d is angular frequency of the tides, ω_m is angular frequency of the spring-neap (14.7 day) cycle, and t is time.

2.2 Hydrodynamic model (HDM)

The design of the aerofoil is dependent on the turbine type and met-ocean condition. The blade element momentum theory (BEMT) code adopted here for blade design and to predict performance of HATT blades is based on previous work [27-29]. A stream-tube model (Figure 2) based on BEMT is employed to calculate steady loads on the turbine blades and the thrust and power of the rotor for varying fluid velocities, rotational speeds and pitch angles. Optimised chord and pitch angle distributions can be defined along the span of the blade for a given set of input parameters (Table 1) [5].

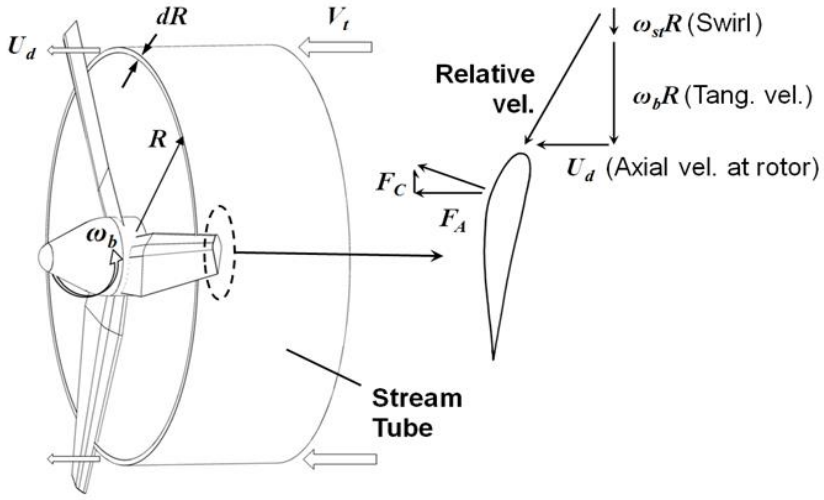

Figure 2. Stream-tube model.

The stream tube model examines a series of concentric tubes, dividing the blade into a number of sections, within which momentum is conserved, as it is transferred from the water to the blade. The BEMT-related mathematical formulation of the forces acting on the blade is given in Appendix 1. The input data for the HDM in this study is given in Table 1.

Table 1. Hydrodynamic model parameters.

Parameter	**Value**
Water Velocity	2.5 m/s
Water density	1025 kg/m³
Water viscosity	0.0013155 Ns/m²
Number of blades	3
Revolutions per minute	16
R_{outer}	5.0 m
R_{inner}	1.5 m
C_L	1.0
L/D	70
Angle of attack	7°
Z	0.333

The design of the aerofoil, viz. chord and twist distribution along the blade, is intended to achieve optimum performance over turbine lifetime. The design code of this paper performs adjustments to the chord length until moment balance is achieved, after which the process is repeated for all remaining stream tubes. The outputs at each radial increment are chord length, aerofoil pitch angle, the axial and tangential force on the blade at particular radial increment, torque, and power.

In order to regulate the turbine power during high water velocity, control systems are used to manage forces and moments on the tidal blade. The HDM is used to simulate the two options for controlling power, pitch- (PR) and stall-regulation (SR). PR is a system which modifies the lift coefficient (C_L), i.e. the forces on the blade, by rotating the entire blade about its axis. SR blades are designed with a radial variation of pitch angle so that, as the tidal velocity increases, the angle of attack over a section of the blade exceeds the stall angle and lift drops off, reducing the forces on the blade [30]. TT blades have a smaller operational range of velocity, typically 0.75 to 3m/s (exceptionally 4m/s), than WT blades [2, 31]. Therefore, the simpler control systems may be viable for tidal turbines. For this study the operational environment is such that both control systems produce the same flapwise moment [32].

The maximum theoretical power levels for SR and PR turbines are calculated and the energy produced by each turbine per year is predicted using HDM (Appendix 1). In order to compare the blade damage accumulation on two turbines with different control systems, the energy output is matched. Hence, the aim was to find the tidal current speed at which the energy output of the PR turbine is similar to that of the SR turbine, to enable an objective comparison with respect to damage accumulation. This is achieved by identifying the threshold value of water velocity for pitch control, above which blade pitch is controlled to give constant power. Figures 3a and 3b show the power curves for a PR tidal turbine (green) and an SR constant speed turbine (blue). Hence, at 3.05m/s current speed these turbines are determined to have similar energy output in a year, with a power rating is approximately 500kW.

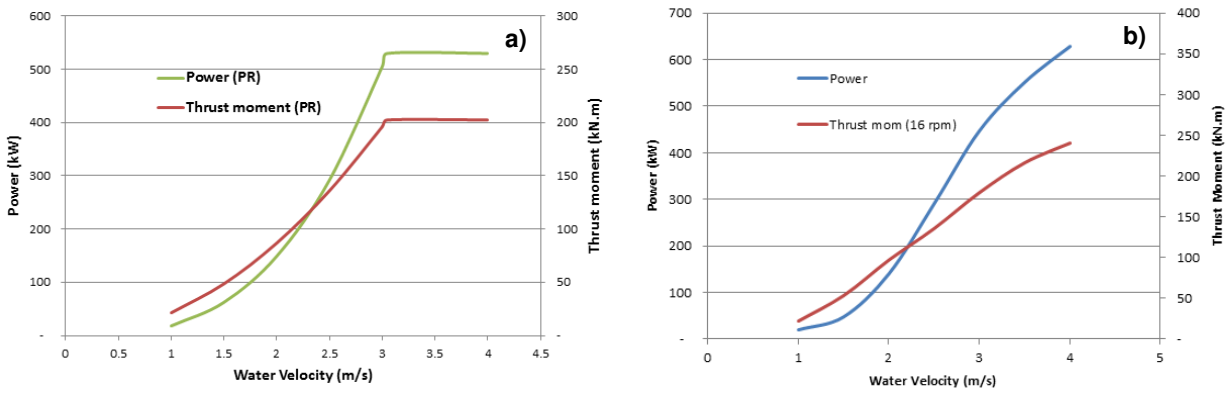

Figure 3. The power curve and thrust moment curve for: a) a pitch-regulated (PR) and b) a stall-regulated (SR) tidal turbine.

176

177 **2.3 Structural model**

178 The structural design of TTBs is governed by the hydrodynamic shape of the aerofoil and the
179 extreme loading conditions. The design of an optimised composite TTB requires several iterations
180 between material characterisation, structural analysis and fluid-structure interaction [4].

181 The blade cross-sections are selected from the family of shapes that provides the best lift-drag
182 characteristics [33], which are fairly thin. However, the blade needs to support a complex combination
183 of loading, including lift, drag, buoyancy, and gravitational forces. These structural requirements lead
184 to the thicker aerofoil than the hydrodynamic optimum requires [34]. For this study RISO-A1-24 (chord
185 thickness is 24% of chord length) is identified as the appropriate aerofoil shape for tidal application
186 [35-37]. The data available for the Risø-A1-24 aerofoil covers a broad range of incidence angles [38].
187 Hence, the choice of aerofoil is based on hydrodynamic performance and structural characteristics
188 (Figure 4a).

189 The study examines the fatigue life of a 5.0 m rotor radius, 3-bladed downstream, free-yaw
190 turbine, which produces approximately 330 kW (operating in a 2.5 m/s tidal current velocity). The
191 HDM uses 45 stream tubes, uniformly distributed along the blade, and assumes that the water in each
192 of these tubes has slowed to 1/3 its initial velocity at the exit ($\zeta = 0.333$). The radial distribution of blade
193 chord length, pitch angle, tangential (torque, F_C), and axial (thrust, F_A) forces is determined by the HDM
194 (Appendix 1) for the set of parameters in Table 1. The chord length at the blade root is 1.25 m with a
195 pitch angle of 20°, while the chord length at the tip is 0.75 m with a pitch angle of 4°. The aerofoil
196 shape has been simplified in the structural model (Figure 4b). F_A increases linearly with increasing
197 radius, from 0.7 kN to 2.3 kN at the extreme blade radius, and is significantly larger than the (power-
198 generating) F_C, which increases with radius from 320 N to 410 N at the extreme blade radius. These
199 forces cause a flapwise bending moment of 150 kNm and edgewise bending moment of 35.7 kNm,
200 respectively, at a 1.5 m radius from the rotor centre. A finite element (FE) model of a TTB has been
201 created using Abaqus FEA software [39] (Figure 4c).

202

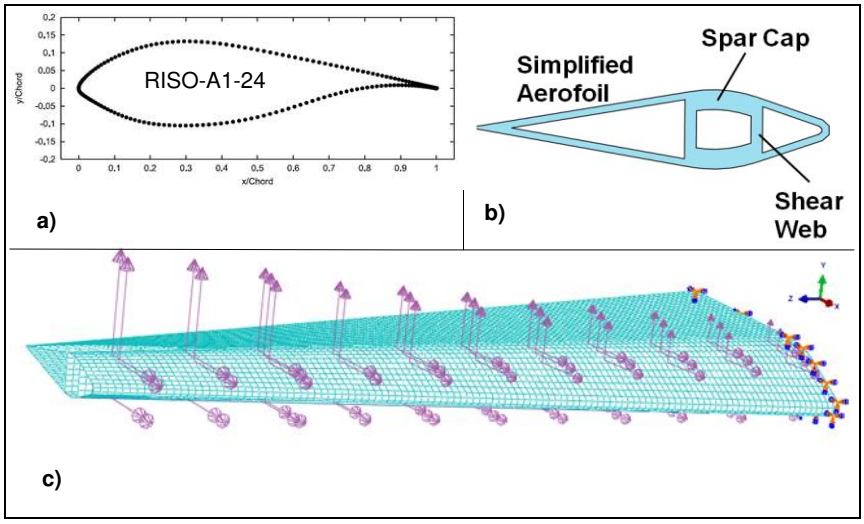

Figure 4. Tidal blade modelling: a) Riso A1-24 cross-section [35], b) simplified aerofoil shape used for final element (FE) analysis, and c) 5 m long tidal turbine blade FE model with applied loading.

The parts of the structure bearing the loads and moments (the spar caps) are separated as far apart as aerofoil geometry enables, but joined together by two shear webs, creating the box section (the main structural element of the blade). The top caps of this box are 35 mm thick at the root and taper to 6 mm at the tip. The shear webs and fairings are 12 mm thick and taper to 4 mm at the tip. In the FE model, the panels of the blade are modelled as shell elements with quasi-isotropic (QI) material properties obtained from the standard laminate analysis [40, 41]. The material characteristics for this study are summarised in Table 2. High-stress locations near the surface are modelled with individual plies for which properties are calculated from the Rule of Mixtures and the Halpin–Tsai equations [42].

Table 2. Tidal blade glass fibre/epoxy material properties.

Inputs		**Single unidirectional ply properties**		**Quasi-isotropic laminate $[(45\backslash 135\backslash 90\backslash 0)_2]_s$**	
V_f	50%	E_1	38 GPa	E_x, E_y	19.3 GPa
E_f	72.4 GPa	E_2	11.6 GPa	G_{xy}	7.2 GPa
v_f	0.22	G_{12}	3.5 GPa	v_{xy}	0.330
E_m	3.5 GPa	v_{12}	0.285		
v_m	0.35				

3. Experimental method

3.1 Coupon manufacture

QI laminates were manufactured using the Vacuum Assisted Resin Transfer Moulding (VARTM) process [43]. Biaxial stitched glass-fibre mat (0°-300 g/m^2, 90°-300 g/m^2) was cut and stacked to create a $[(45/135/90/0)_2]_S$ laminate and epoxy resins were infiltrated under vacuum (Figure 5). The laminates were cured for 48 hours at room temperature and then post-cured for 5 hours at 80° C in an oven. The average thickness of the laminate is 3.75 mm with 50% fibre volume fraction. The laminates were cut into 25 mm × 250 mm coupons for testing.

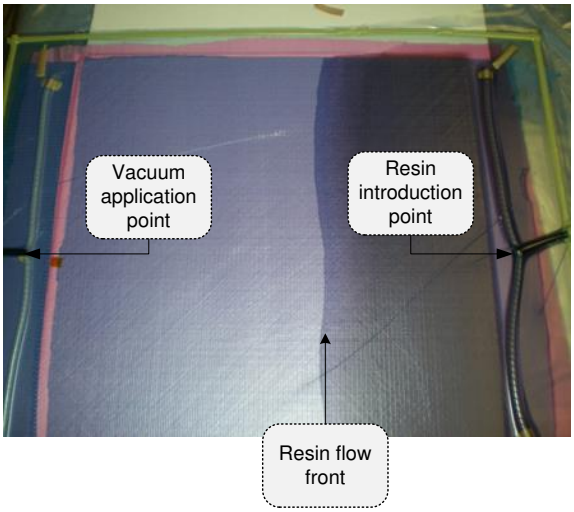

Figure 5. Laminate manufacturing using vacuum assisted resin transfer moulding (VARTM) [43].

3.2 Accelerated ageing procedure

The total number of test coupons for material fatigue testing was ten. Five of these were acceleration-aged in warm water (30° to 40°) for up to 2.5 years (900 days) to simulate immersion in 12° C seawater for approximately 20 years. The rest were stored at normal room temperature and humidity for a similar length of time. Thus, by increasing the water temperature, movement of moisture by diffusion into the polymer resin within the composite is accelerated. The diffusion rate (k_d) varies with temperature (Arrhenius law):

$$k_d = k_0 e^{-\frac{E}{RT}} \tag{2}$$

where k_0 is the reference diffusion rate coefficient, E is the activation energy, R is the universal gas constant (8.3145 kJ kmol^{-1}K^{-1}), and T is the temperature (K). An acceleration factor, for a higher temperature in the same material, has been defined as [44]:

$$F_{H,L} = e^{-\left[\frac{E}{R}\left(\frac{1}{T_H}-\frac{1}{T_{ref}}\right)\right]} \quad (3)$$

Selection of the higher temperature (T_H) to produce a required acceleration factor relative to a given reference (T_{Href}) temperature depends on the value of the activation energy (E), taken here as 93 kJ kmol^{-1} for epoxy/E-glass composite [44, 45]. Figure 6 shows a plot of the acceleration factors for epoxy versus aging water temperature. For a tidal turbine operating off the coast of Ireland, the design operating temperature (T_{ref}) is 12°. The figure shows that at 30°C ageing temperature, the acceleration factor is approximately 10 and at room temperature (20°C) it is approximately 3, when compared to the 12°C operating environment.

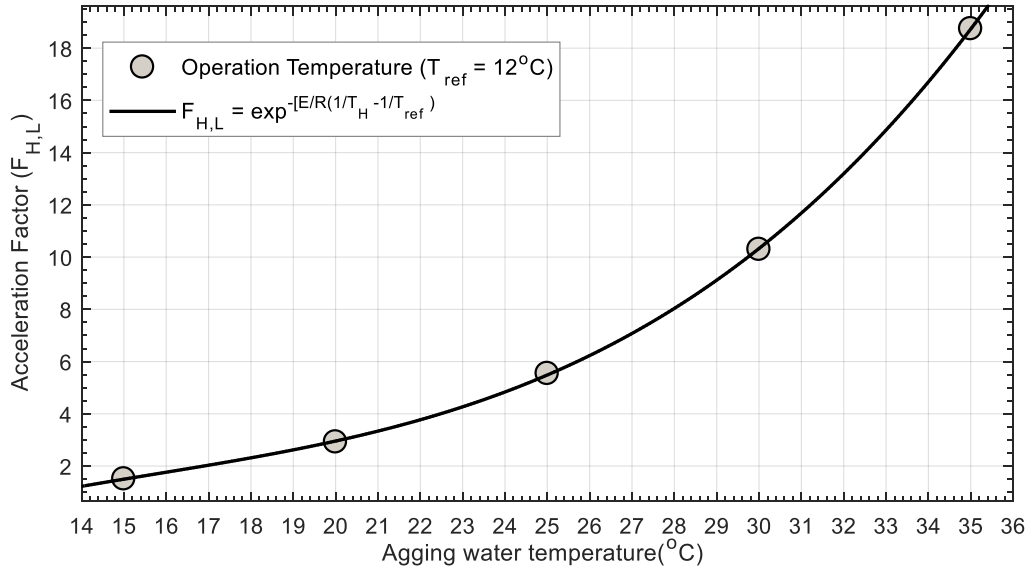

Figure 6. Anticipated acceleration factor for epoxy/E-glass composite due to ageing using elevated water temperature.

Two containers were filled with tap water and equipped with heater-stirrer units to ensure that the heated water is circulated throughout the entire tank (Figure 7a). The water bath temperature was controlled by a heater and thermometer. The epoxy/E-glass coupons were immersed in baths and maintained at 20°C (unheated tank) and 30°C ± 1°C (heated tank). The coupons are stacked on an aluminium plate in the bottom of the bath in a way that allows maximum water circulation around the coupons while supporting the coupons evenly, to prevent stressing of the coupons during the aging process. Before placement in the tank, the coupons were weighed and the weight recorded to a resolution of 0.001 g. The average weight for the epoxy/E-glass coupons was 43.872 g with a variation

of up to 4.1%. To measure the amount of water absorbed, the coupons were re-weighed at intervals during the immersion ageing process.

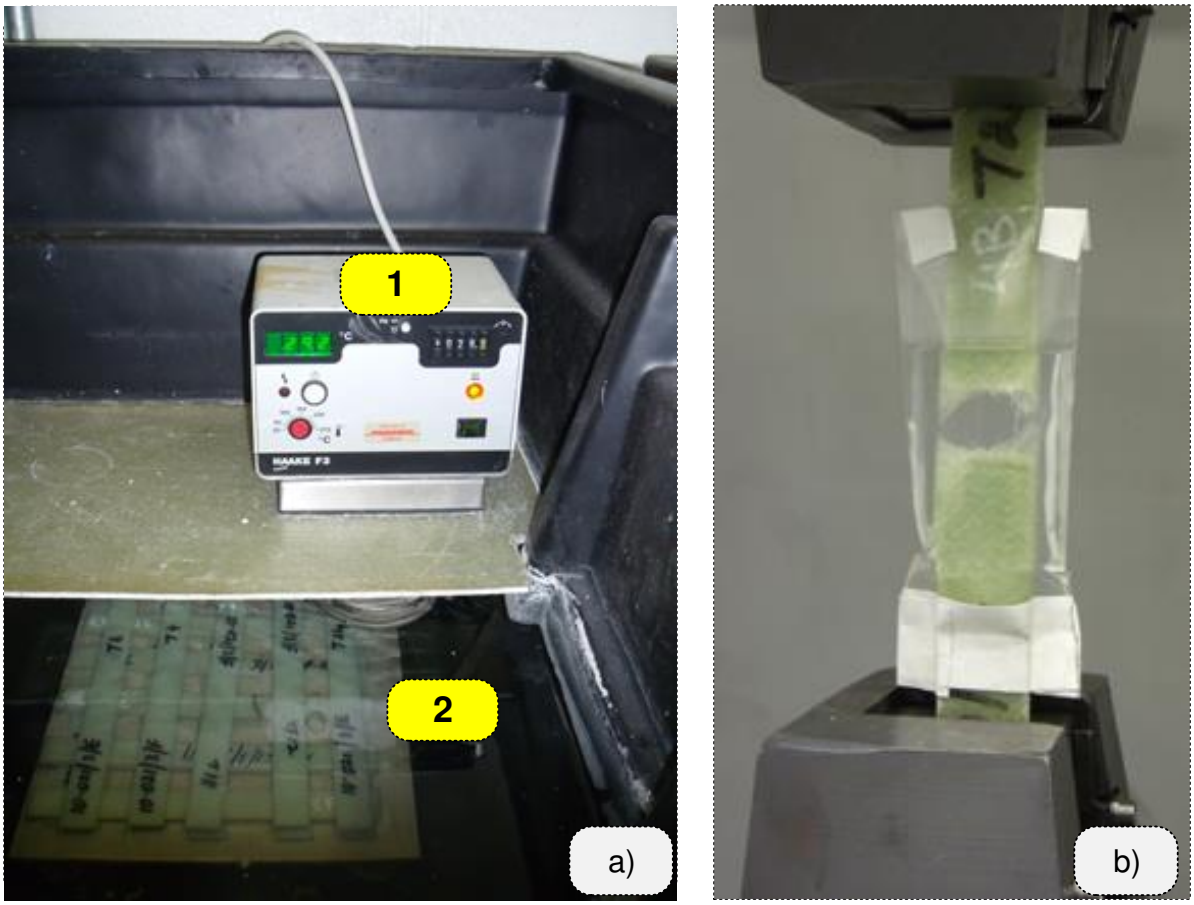

Figure 7. a) Setup of the ageing water baths: 1. Heater-stirrers used to maintain constant uniform temperature in immersed ageing water baths and 2. Immersed Epoxy / E-glass coupons; b) Immersed fatigue test setup, polyethene pouch with waterproof tape.

3.3 Fatigue test method

Fibre orientation and volume fraction (V_f) are primary determinants of the static and fatigue strength of a composite [40]. The progressive fatigue zone starts at approximately 80% of ultimate tensile strength (UTS), which corresponds to around 1000 cycles and reduces to approximately 25% at over 1 million cycles [46]. Fatigue tests were performed with an Instron 8500 test machine and 8800 controller, applying a sinusoidal force in tension-tension mode ($R = 0.1$) between 3 and 6 Hz. To ensure that the coupon does not overheat, the fatigue test frequency is decreased to enable a constant rate of strain application. After the immersion-aged period, the coupons are subjected to sample initial tests to develop the test setup. Studies show that epoxy composites recover most of their original strength when they are re-dried after water saturation [11, 47]. In order to keep the samples immersed during the

fatigue test, a plastic bag pouch sealed with waterproof tape was used to protect the specimens from drying (Figure 7b). The majority of the fatigue testing was carried out at a constant amplitude in tension-tension (R = 0.1) mode. However, some coupons were exposed to fatigue cycling between 15.5 MPa and 155 MPa for 10^4 cycles, after which they were tested to failure in a constant amplitude (R = 0.1) fatigue test to 180 MPa maximum stress. A power-law relationship (Coffin-Manson equation) is adopted, relating maximum applied strain ($\epsilon_{max,i}$) and fatigue life:

$$\epsilon_{max,i} = AN_f^{-B} \tag{4}$$

where N_f is the number of cycles to failure, and A and B are constants.

4. Fatigue Life Model

The focus of the fatigue model is the highest tensile strain in the blade, caused predominantly by bending. Each tidal cycle causes anincrease and then a decrease in the maximum strain on the blade. Concurrently, for each revolution of the device, the blade experiences a cyclic load caused by the blocking ('shadow') effect of the support tower. The tower reduces the water velocity downstream leading to a brief reduction in the lift force and bending moment on the blades in every cycle. [8, 23] (Figure 8).Wave interaction can also lead to fluctuations in the load on TTBs [3]. The testing of TTs in wave tanks has found flapwise bending moment amplitude reductions of 50% [48, 49] due to tower shadow. In this study, a reduction of 50% of TTB bending moment is considered which corresponds to a fatigue loading R-ratio ($\varepsilon_{min}/\varepsilon_{max}$) of 0.5, as shown in Figure 8.

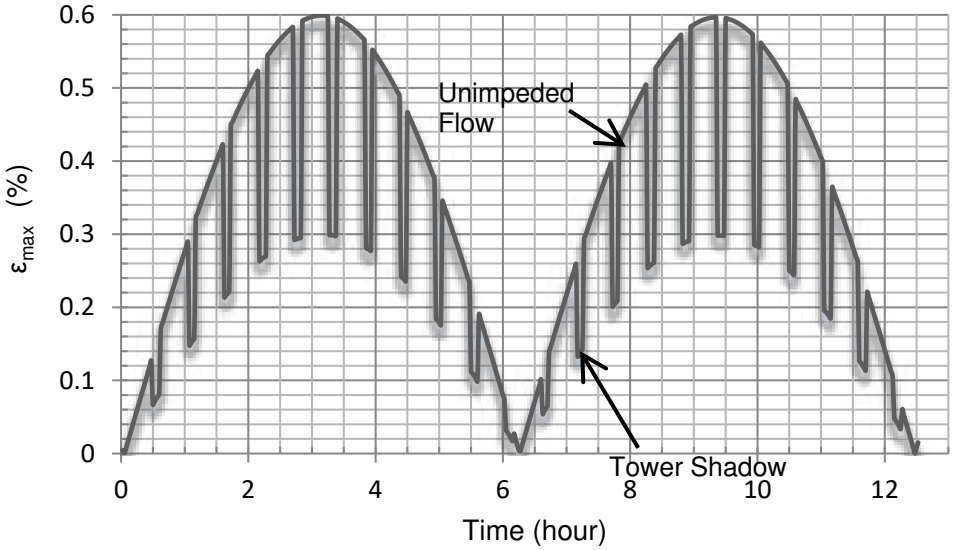

Figure 8. The effect of tower shadow on the maximum strain in the turbine blade (simplified representation).

There is no generally accepted method for dealing with the effect of mean stress in fatigue of composites, i.e. for inferring the ε-N curves from one (test) R-ratio to a different R-ratio [50]. Therefore, to deduce the R=-1.0 and R=0.5 ε-N data from the (measured) R=0.1 data, the method described in [51] is used, based on the constant life diagrams (CLD) assumed behaviour:

1) The N_f= 5000 line joins the R = 0.1 test data point to the material ultimate strain, ε_u, data point on the mean strain axis.
2) For -1 ≤ R ≤ 0.5, the constant life lines (CLL) are parallel to the N_f= 5000 line, based on experimental observations.
3) For R > 0.5, the CLLs join the R = 0.5 data points to the ε_u data point on the mean strain axis.

The material of the turbine blade is linearly elastic, hence the major strains in the blade are directly proportional to the flapwise bending moment, accordingly the maximum strain at any time j is:

$$\varepsilon_{max,j} = \varepsilon_{max,sp}\left(\frac{M_f(v_j)}{M_{ref}}\right)^2 \quad (5)$$

where $M_f(v_j)$ represents the functional dependence of bending moment on tidal current velocity, M_{ref} is the reference bending moment and ε_{ref} is the maximum strain in the blade when the reference moment is applied corresponding to a specific reference velocity V_{ref}.

The fatigue model has two components: I) sums the damage due to the strain cycles caused by the low-frequency semi-diurnal tidal cycle, and II) caused by the higher frequency cycles, due to the tower shadow effect. The fatigue model obtains the tidal velocity from equation (1) and the maximum strain in the blade during that revolution, equation (5). Equation (4), for the observed strain level, determines the number of cycles to failure. For a particular integration point in the FE model of the blade, the damage fractions are summed to find the 7-day damage and hence the turbine life, using a Miner's rule approach [52]:

$$D_{7-day} = \sum_{k,tide}^{N_{7-day}} \frac{1}{N_{f,k}} + \sum_{j,rev}^{N_{7-day}} \frac{1}{N_{f,j}} \quad (6)$$

where N_k is the number of tidal movements during the 7-day period, N_j is the number of turbine revolutions during the 7-day period, $N_{f,k}$ and $N_{f,j}$ are the numbers of cycles to failure for a given combination of mean and alternating strain during each tide and revolution, respectively, k is the increment of tidal cycles, and j is the increment of revolutions of the turbine. Hence, the blade life in years is:

$$Blade\ life_{years} = \frac{7.38}{365.25 D_{7-day}} \quad (7)$$

where 7.38 is the exact length of the 7-day period used (1/4 of a synodic month) and 365.25 the length of a year in days.

5. Results and Discussion

5.1 Water uptake during the immersion-aging period

The percentage weight of water absorbed by the epoxy/E-glass coupons immersed in the ageing tanks at 30°C and at 20°C (room temperature) is shown in Figure 9. The higher temperature has enabled the coupons immersed at 30°C to absorb water more quickly and become saturated at approximately 0.60% moisture. In comparison, the coupons at 20°C had not become saturated by the end of the immersion period (30 months). However, the percentage of moisture absorbed by the epoxy composite coupons in this study is amongst the lowest reported in the literature [53]. There are two reasons: 1) the particular polymers are designed for use in immersed applications, , and 2) the laminates from which the coupons were taken had a low void content (0.22% void content measured in the epoxy/E-glass).

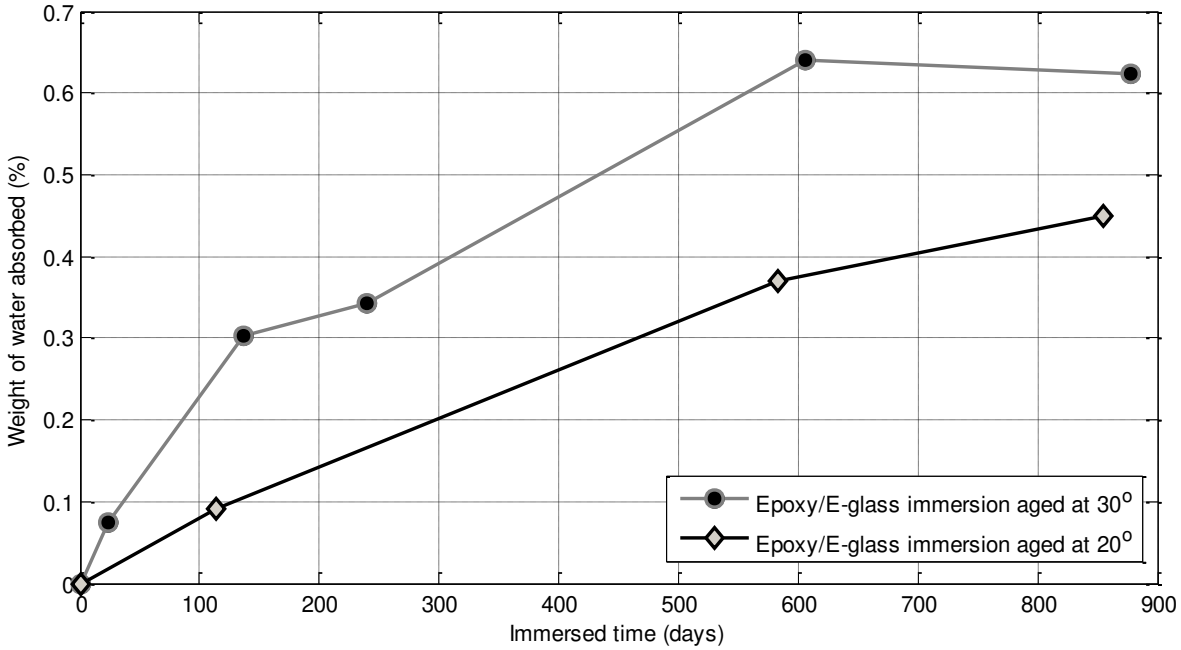

Figure 9. The weight of water absorbed by Epoxy/E-glass composite specimens during water immersion ageing.

5.2 Fatigue test results

The stress-life fatigue testing results for wet and dry epoxy/E-glass QI coupons in tension-tension mode (R = 0.1) are shown in Figure 10. The dry coupons are tested at room temperature (20°C). The wet coupons immersed for 30 months in 30°C water are tested while immersed in water at 20°C. All the immersed coupons broke in the zone of immersion within the pouch during fatigue testing. It is important to keep the coupons wet during testing for the best representation of the immersed failure condition, as any drying that takes place during the testing tends to be accompanied by a recovery in strength [54]. The water aged and immersed coupons show a significant decrease in fatigue strength compared to the dry air aged coupons. The wet aged fatigue strength decreases by 20 to 25% at high stresses, while the wet aged strength is 8% below the fatigue strength of the dry material at high cycles. Hence, the effect of water saturation on the fatigue strength of QI GFRP is stress level dependent. Therefore, the fatigue life reduction of an immersed structure will depend on the spectrum of fatigue stress cycles it experiences while in service.

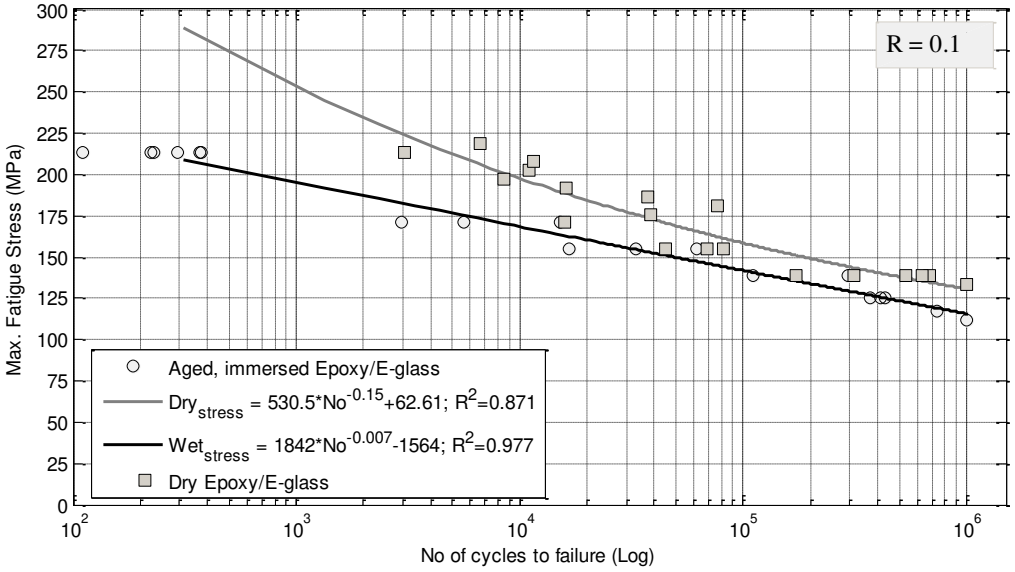

Figure 10. Stress-life curves for wet and dry epoxy/E-glass in R = 0.1 fatigue tests.

5.3 Damage model results

The SN curves generated using damage model predictions of fatigue life for a range of constant amplitude fatigue stresses in both wet and dry QI epoxy/E-glass laminates are shown in Figure 11. The model successfully predicts the stress dependence of the fatigue strength degradation due to water saturation. There is good agreement between the prediction and the experimental findings: a 20% reduction in fatigue strength due to water immersion at a fatigue life of 1,000 cycles.

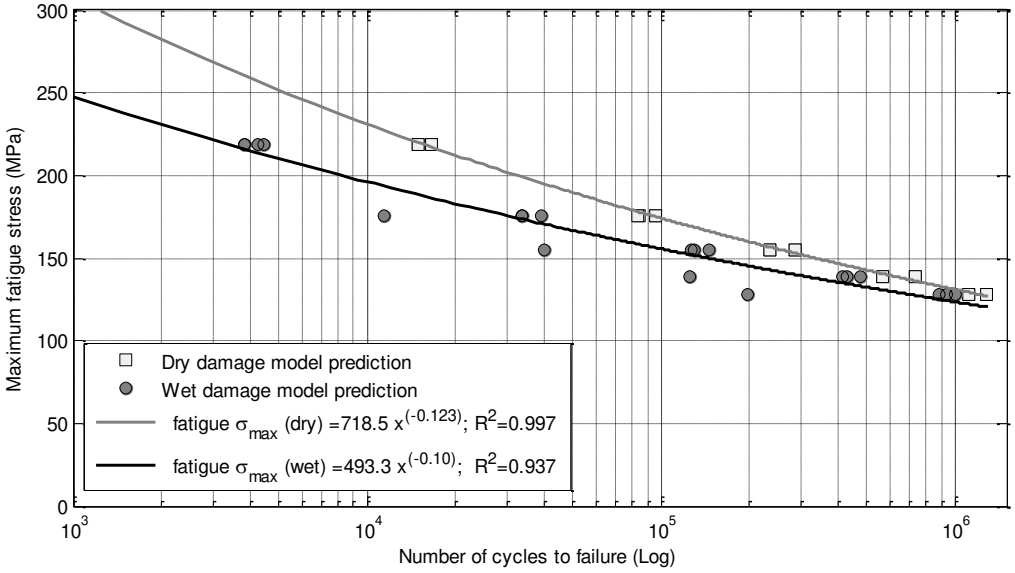

Figure 11. Damage model predictions for wet and dry stress-life curves of QI epoxy / E-glass coupons in constant amplitude fatigue.

5.4 Fatigue life with tidal turbine blade stress spectrum

The predicted fatigue lives of Stall-Regulated (SR) and Pitch-Regulated (PR) TTBs and corresponding fitting curves are plotted against maximum stress experienced by the blade when the tidal flow is 2.5 m/s (Figure 12). The results for the PR turbine shows that a blade with a maximum stress of 72 MPa, which is predicted to have a 5 year "dry" life, will fail, on average, 1.7 years earlier if the blade laminates are water saturated. If the thickness of the laminate is increased to reduce the stresses in the blade to 63.5 MPa, the "dry" life becomes 20 years and the "wet" life decreases to 19.1 years when water saturated. This convergence of the wet and dry laminate lives occurs because pitch regulation limits the maximum stress in the blades. In achieving the longer blade fatigue life (>15 years), stresses are limited to levels where the difference in life between wet and dry laminates is very small.

The predicted 20 years "dry" fatigue life of an SR TTB is reduced to 17 years if the laminate is water saturated. Furthermore, if the maximum stress in the blade is 66 MPa, then the predicted "dry" life is 5 years and the predicted "wet" life is 2.9 years. In general, the life of water saturated blades is reduced approximately 3 years and 1–2 years for SR and PR turbines, respectively. Hence, the laminates would need to be 1 to 4% thicker to counteract the effects of water saturation on the blade.

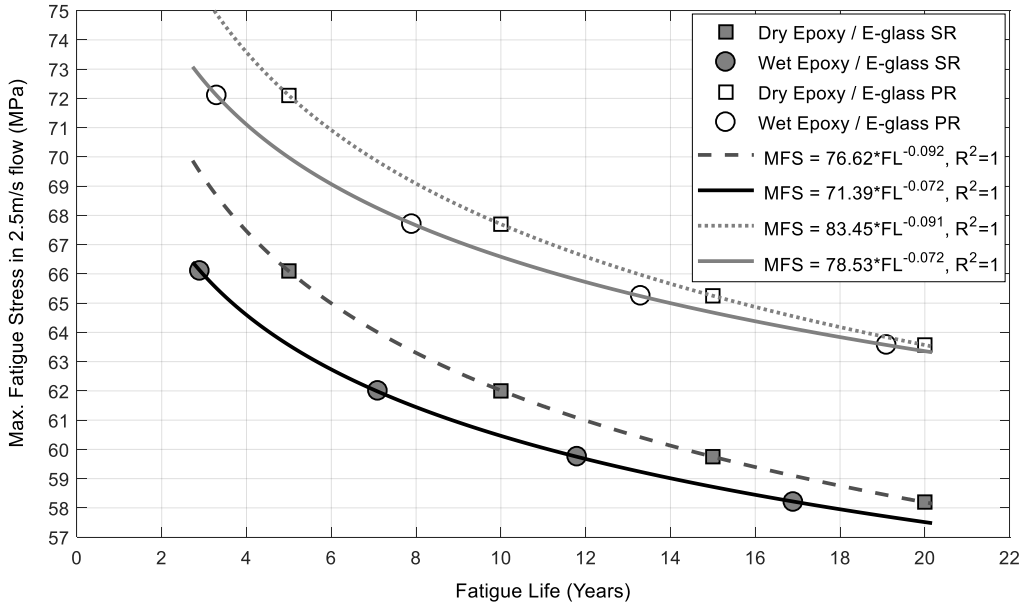

Figure 12. Effect of seawater immersion on predicted fatigue life of pitch-regulated (PR) and stall-regulated (SR) tidal turbine blades.

5.5 Blade Finite Element analysis

Figure 13 shows the deflection obtained using an FEA model of the blade (root area excluded) exposed to factored loading (safety factor = 2). The deflection of the tip is 334 mm (approx. twice the blade aerofoil thickness at the tip) and does not introduce any significant error into the structural and hydrodynamic calculations.

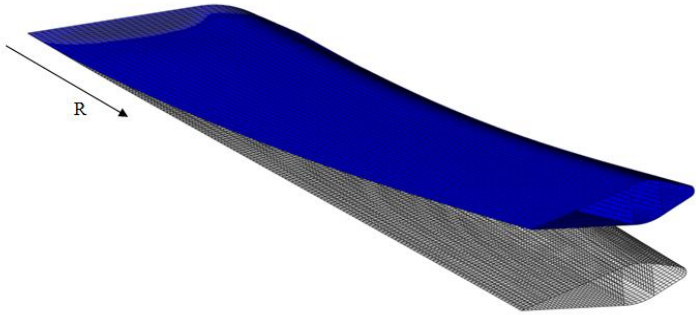

Figure 13. The undeformed and deformed shape of the blade at 2.5m/s water velocity, with a factor of safety of 2.0 applied.

As expected, the highest stresses and strains occur near the root, in the spar caps of the structural beam box section (Figure 14). These are primarily caused by the large (flapwise) bending moments due to the thrust force.

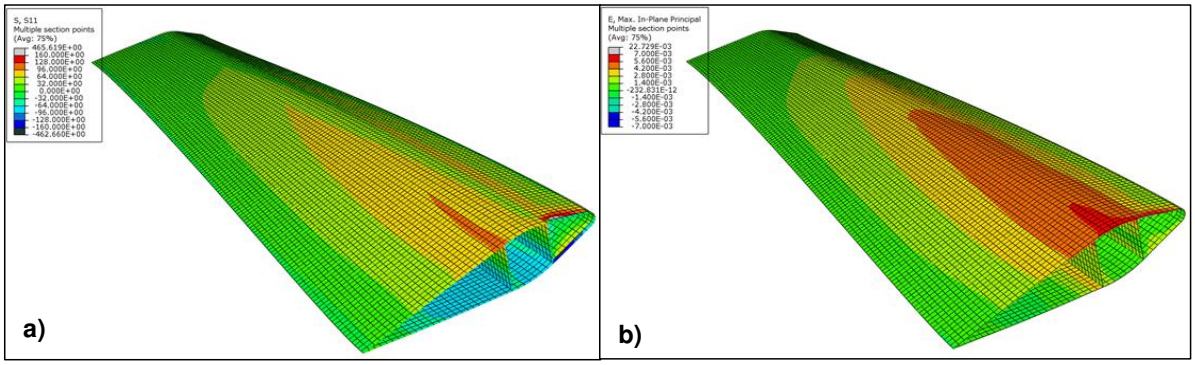

Figure 14. a) Fibre direction stresses in 45° surface ply under design load. b) Maximum principal strains in the outer surface under design load.

The maximum bending strains occur on the outer surface and the maximum principal strains in the middle of the spar cap. Since the surface ply is at 45° to the blade axis, it is necessary to find the maximum fibre strain in a ply in which the fibres are closely aligned to the load direction in order to make an appropriate comparison to the experimental fatigue life data. Figure 15 shows a plot of fibre strains along a section through the midline of the pressure side spar cap extending from near the hub to the tip of the blade. The fibres in the three outermost plies are at 45°, 135° and 90° to the blade axis

436 which reduces their fibre strains. The 4th ply from the surface has its fibres at 0° to the blade axis (i.e.
437 aligned with the direction of the principal bending strains). Hence, the maximum fibre strains are
438 predicted in this ply.
439

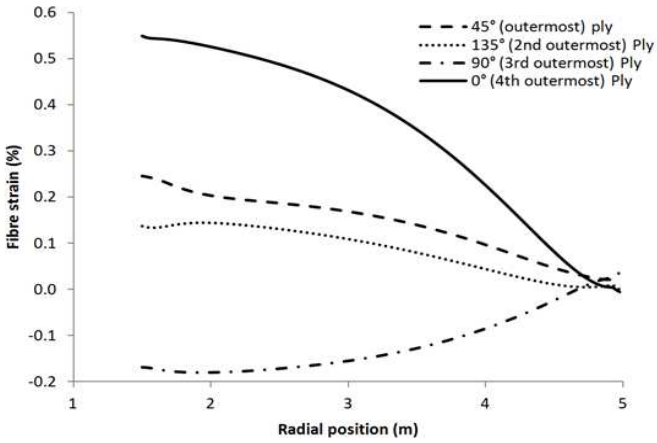

440
441 Figure 15. Fibre strains in the four outermost plies at maximum strain locations along blade
442 operating in 2.5 m/s water velocity.
443
444 The maximum fibre strain in the blade at 2.5 m/s water velocity is used to calculate maximum
445 fibre strain at any water velocity given the flapwise bending moment at that water velocity and the
446 assumption of linear elasticity in the blade using Equation 5. By integrating over the tidal pattern
447 predicted maximum theoretical power levels for both PR and SR turbines, obtained by HDM, the energy
448 produced by each turbine per year is calculated. In order to compare the PR and SR turbines with respect
449 to fatigue damage accumulation, the energy output from the PR turbine is matched to that of the SR
450 turbine. This is achieved by identifying the threshold value of water velocity for pitch control, above
451 which blade pitch is controlled to give constant flapwise moment (power). Using HDM for the PR
452 turbine, the threshold water velocity value is found to be 3.05 m/s.
453
454 **5.6 Blade fatigue life and energy production**
455 In order to predict fatigue damage accumulation (Equations 4-6), the moment-velocity
456 relationships are fitted with polynomial expressions, to allow interpolation with respect to water
457 velocity. The fatigue model used to analyse the case given in Table 3 predicted a fatigue life of 11.6
458 years. The fatigue life model can be employed to study the effect of each of the parameters on the blade
459 fatigue life [23].
460
461
462 Table 3. Parameters for fatigue reference case.

Parameter	Value
Water Velocity	4.0m/s
Neap max. velocity / Spring max. velocity	60%
Factor of safety applied to loads	2
Tower shadow	50%
Control system	PR

To compare the fatigue life of SR and PR turbine blades, the fatigue damage fraction for each rotation of the turbine is sorted into bins for 0.1 m/s increments of water velocity, as shown in Figure 16a (note that the area under each curve, which represents total accumulated damage over the blade lifetime, is equal to 1.0). The SR blade accumulates a lot of damage at high water velocities, due to the higher bending strains, whereas for the PR blade, the damage at high velocities is significantly lower, due to the lower bending strains. Most of the PR blade damage is sustained at medium water velocities, due to the greater number of operational hours in this regime. The fatigue model predicts that a blade which survives 20 years on the PR device will only survive 12.8 years on the SR device. On the other hand, if the laminates in the spar cap of the blade are increased by just 10% it would survive 22 years on the SR machine. An increase in water velocity will not reduce blade life because the blades will feather at maximum power either way.

Figure 16b shows energy capture for different control systems (note: the stall characteristics and the pitch regulating point of the corresponding blades were chosen to give the same energy capture over the 20-year design life). If the maximum or average speeds at the turbine site do not match the design speed of the turbine it can have significant impacts on energy production or the life of SR turbine. A 10% decrease in the velocity of tidal flows will reduce energy production per year by 20%, whereas a 10% increase in tidal speed will reduce life from 20 to 12.1 years. In this situation, the PR turbine would not experience the same reduction in energy production as the SR turbine. There will be some loss in energy produced because the average will be lower, but looking at the bins data it can be seen that only 1/4 of the energy is produced before the pitch regulation point and will be affected by the loss in speed, above this point the turbine will make the same power either way.

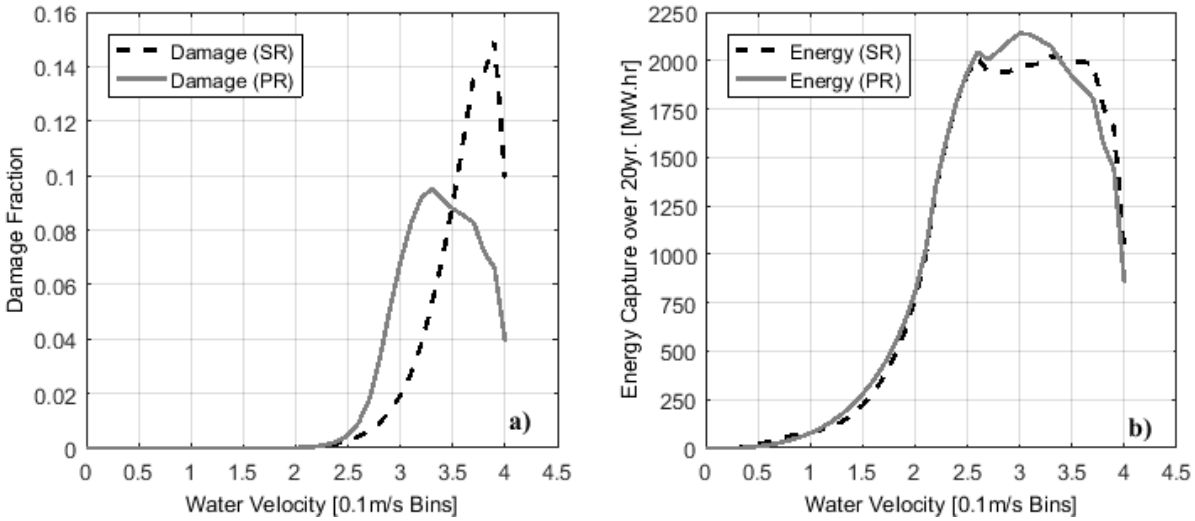

Figure 16. Stall- and pitch-regulated tidal turbine blades: a) damage fraction and b) energy capture for different water velocities.

6. Conclusion

A preliminary design and fatigue life assessment methodology for composite tidal turbine blades (TTBs) is used to compare the predicted fatigue life of pitch-regulated (PR) and stall-regulated (SR) tidal turbine devices. The immersion of GFRP materials in 12°C seawater for a period of 20 years is simulated by immersing specimens in warm water (30°C) for approximately 2.5 years, showing that the coupons absorbed relatively small amounts of water (0.2% to 0.6%) due to the characteristics of chosen material and fabrication procedures adopted. The fatigue strength of the aged-water-immersed material is stress-level dependant and is significantly reduced, showing 20% and 8% reduction for a fatigue life of 10^3 cycles and 10^6 cycles, respectively, in comparison with the dry samples.

It was found that the life of water-saturated blades is reduced by about 3 years and 1–2 years for SR and PR turbines, respectively. In order to neutralise the effect of the water saturation, the laminates need to be thicker by 1-4%. The study of SR and PR TTBs based on same energy capture over the 20-year design life found that blades on an SR tidal turbine need approximately 10% thicker laminates than those on a PR turbine for a given design fatigue life.

The results of this study were encouraging for the future development of more advanced fatigue analysis and design methodologies for tidal turbine blades, which will include more structural details (e.g. root connections, stress concentration at ply drops and holes, etc.), more comprehensive material modelling (e.g. modelling of individual plies with associated orientations) and more realistic water velocity conditions (e.g. effect of turbulence and wave-loading).

Acknowledgements

The authors would like to acknowledge funding from Science Foundation Ireland (SFI) through the Advance Award (14/ADV/RC3022) and the Marine and Renewable Energy Ireland (MaREI) Centre, Grant No. 12/RC/2305; and from the European Union under Framework 7, through the MARINCOMP Project, Grant agreement no.: FP7-612531.

References

[1] F. O Rourke, F. Boyle, and A. Reynolds, "Tidal energy update 2009," *Applied Energy,* vol. 87, pp. 398-409, 2// 2010.

[2] F. O'Rourke, F. Boyle, and A. Reynolds, "Tidal current energy resource assessment in Ireland: Current status and future update," *Renewable and Sustainable Energy Reviews,* vol. 14, pp. 3206-3212, 2010.

[3] E. M. Fagan, C. R. Kennedy, S. B. Leen, and J. Goggins, "Damage mechanics based design methodology for tidal current turbine composite blades," *Renewable Energy,* vol. 97, pp. 358-372, 11// 2016.

[4] P. Davies, G. Germain, B. Gaurier, A. Boisseau, and D. Perreux, "Evaluation of the durability of composite tidal turbine blades," *Philosophical Transactions of the Royal Society of London A: Mathematical, Physical and Engineering Sciences,* vol. 371, 2013-02-28 00:00:00 2013.

[5] D. Grogan, S. Leen, C. Kennedy, and C. O. Brádaigh, "Design of composite tidal turbine blades," *Renewable Energy,* vol. 57, pp. 151-162, 2013.

[6] I. Munteanu, "Wind turbine control systems. Principles, modelling and gain scheduling design. Fernando D. Bianchi, Hernán De Battista and Ricardo J. Mantz, Springer, London, 2006. No. of pages: XIX+ 207. Price: $119," ed: Wiley Online Library, 2008.

[7] J. F. Manwell, J. G. McGowan, and A. L. Rogers, *Wind energy explained: theory, design and application*: John Wiley & Sons, 2010.

[8] G. S. Bir, M. J. Lawson, and Y. Li, "Structural Design of a Horizontal-Axis Tidal Current Turbine Composite Blade," in *ASME 2011 30th International Conference on Ocean, Offshore and Arctic Engineering*, 2011, pp. 797-808.

[9] G. S. Springer, "Environmental effects on composite materials. Volume 3," 1988.

[10] R. Martin, *Ageing of composites*: Elsevier, 2008.

[11] R. Maurin, Y. Perrot, A. Bourmaud, P. Davies, and C. Baley, "Seawater ageing of low styrene emission resins for marine composites: Mechanical behaviour and nano-indentation studies," *Composites Part A: Applied Science and Manufacturing,* vol. 40, pp. 1024-1032, 8// 2009.

[12] L. Smith and Y. Weitsman, "The immersed fatigue response of polymer composites," *International journal of fracture,* vol. 82, pp. 31-42, 1996.

[13] C. R. Kennedy, S. B. Leen, and C. M. Ó Brádaigh, "Immersed Fatigue Performance of Glass Fibre-Reinforced Composites for Tidal Turbine Blade Applications," *Journal of Bio- and Tribo-Corrosion,* vol. 2, pp. 1-10, 2016.

[14] N. B. Baba, A. S. Suhaimi, M. A. Mohd Amin, and A. Mohd, "Study on Mechanical and Physical Behaviour of Hybrid GFRP," *Advances in Materials Science and Engineering,* vol. 2015, p. 7, 2015.

[15] C. R. Kennedy, C. M. Ó. Brádaigh, and S. B. Leen, "A multiaxial fatigue damage model for fibre reinforced polymer composites," *Composite Structures,* vol. 106, pp. 201-210, 2013.

[16] J. Degrieck and W. Van Paepegem, "Fatigue damage modeling of fibre-reinforced composite materials: Review," *Applied Mechanics Reviews,* vol. 54, pp. 279-300, 2001.

[17] DNV GL – Energy, "Horizontal axis tidal turbines," in *Renewables Certification – Wave and Tidal*, ed, 2014, p. 284.

[18] A. P. Vassilopoulos, B. D. Manshadi, and T. Keller, "Influence of the constant life diagram formulation on the fatigue life prediction of composite materials," *International Journal of Fatigue,* vol. 32, pp. 659-669, 4// 2010.

[19] L. Broutman and S. Sahu, "A new theory to predict cumulative fatigue damage in fiberglass reinforced plastics," in *Composite materials: Testing and design (second conference)*, 1972.

[20] C. Kassapoglou, "Fatigue of composite materials under spectrum loading," *Composites Part A: Applied Science and Manufacturing,* vol. 41, pp. 663-669, 2010.

[21] X. Duan and W. X. Yao, "Multi-directional stiffness degradation induced by matrix cracking in composite laminates," *International Journal of Fatigue,* vol. 24, pp. 119-125, 2// 2002.

[22] R. Talreja, "Continuum modeling of the development of intralaminar cracking in composite laminates," in *ICF7, Houston (USA) 1989*, 2013.

[23] C. R. Kennedy, S. B. Leen, and C. M. Ó. Brádaigh, "A preliminary design methodology for fatigue life prediction of polymer composites for tidal turbine blades," *Proceedings of the Institution of Mechanical Engineers, Part L: Journal of Materials Design and Applications,* p. 1464420712443330, 2012.

[24] T. Shimokawa and S. Tanaka, "A statistical consideration of Miner's rule," *International Journal of Fatigue,* vol. 2, pp. 165-170, 1980/10/01 1980.

[25] R. H. Clark, *Elements of tidal-electric engineering*: John Wiley and Sons, 2007.

[26] A. G. Bryans, B. Fox, P. A. Crossley, and M. O'Malley, "Impact of tidal generation on power system operation in Ireland," *IEEE Transactions on Power Systems,* vol. 20, pp. 2034-2040, 2005.

[27] W. M. J. Batten, A. S. Bahaj, A. F. Molland, and J. R. Chaplin, "The prediction of the hydrodynamic performance of marine current turbines," *Renewable Energy,* vol. 33, pp. 1085-1096, 5// 2008.

[28] A. S. Bahaj, W. M. J. Batten, and G. McCann, "Experimental verifications of numerical predictions for the hydrodynamic performance of horizontal axis marine current turbines," *Renewable Energy,* vol. 32, pp. 2479-2490, 12// 2007.

[29] H. Glauert, "The Elements of Airfoil and Airscrew Theory," ed: Cambridge University Press, 1959.

[30] B. Whitby and C. E. Ugalde-Loo, "Performance of Pitch and Stall Regulated Tidal Stream Turbines," *Sustainable Energy, IEEE Transactions on,* vol. 5, pp. 64-72, 2014.

[31] SEI, "Tidal and Current Energy Resources in Ireland Report," Dublin, Ireland2006.

[32] R. Carr, "Tide height data. (personal communication)," C. R. Kennedy, Ed., ed. Galway, Ireland: The Marine Institute, July, 2010.

[33] UIUC, "Airfoil Data Set," ed. Illinois, USA: University of Illinois at Urbana–Champaign (UIUC), Applied Aerodynamics Group 2016.

[34] E. Hau, "Rotor Blades," in *Wind Turbines: Fundamentals, Technologies, Application, Economics*: Springer Berlin Heidelberg, 2013, pp. 269-304.

[35] F. Bertagnolio, N. N. Sørensen, J. Johansen, and P. Fuglsang, "Wind turbine airfoil catalogue," Riso National Laboratory, Roskilde, Denmark2001.

[36] D. Sale, J. Jonkman, and W. Musial, "Hydrodynamic Optimization Method and Design Code for Stall-Regulated Hydrokinetic Turbine Rotors," NREL2009.

[37] M. R. Ahmed, "Blade sections for wind turbine and tidal current turbine applications–current status and future challenges," *International Journal of Energy Research,* vol. 36, pp. 829-844, 2012.

[38] P. Fuglsang, I. Antoniou, and K. S. Dahl, *Wind Tunnel Tests of the Risø-A1-18, Risø-A1-21 and Risø-A1-24 Airfoils*: Risø National Laboratory, 1999.

[39] SIMULIA. (2010). *"Abaqus FEA". Dassault Systèmes*. Available: http://www.3ds.com/products-services/simulia/products/

[40] I. M. Daniel and O. Ishai, *Engineering Mechanics of Composite Materials*: Oxford University Press, USA, 1994.

[41] Pipes R . Byron, Carlsson A . Leif, and Adams F . Donald, *Experimental Characterization of Advanced Composite Materials*, 4th ed. Boca Raton, USA: Taylor & Francis Group, LLC, 2014.

[42] B. D. Agarwal, L. J. Broutman, and K. Chandrashekhara, *Analysis and performance of fiber composites*: John Wiley & Sons, 2006.

[43] B. T. Åström, *Manufacturing of Polymer Composites*. London, UK: Chapman & Hall, London, 1997.

[44] P. Purnell, J. Cain, P. Van Itterbeeck, and J. Lesko, "Service life modelling of fibre composites: A unified approach," *Composites Science and Technology,* vol. 68, pp. 3330-3336, 2008.

[45] C. R. Kennedy, "Fatigue of Glass Fibre Composites in Marine Renewable Energy," Doctor of Philosophy, National University of Ireland, Galway, 2013.

[46] G. Sims, "Fatigue test methods, problems and standards," *Fatigue in composites, in: B. Harris (ed.), Woodhead publishing limited,* pp. 36-63, 2003.

[47] P. Davies, F. Mazeas, and P. Casari, "Sea water aging of glass reinforced composites: shear behaviour and damage modelling," *Journal of composite materials,* vol. 35, pp. 1343-1372, 2001.

[48] I. Shugan, H.-H. Hwung, and R.-Y. Yang, "Wave-current interactions," in *EGU General Assembly Conference Abstracts*, 2012, p. 8263.

[49] N. Barltrop, K. Varyani, A. Grant, D. Clelland, and X. Pham, "Wave-current interactions in marine current turbines," *Proceedings of the Institution of Mechanical Engineers, Part M: Journal of Engineering for the Maritime Environment,* vol. 220, pp. 195-203, 2006.

[50] C. R. Kennedy, S. B. Leen, and C. r. M. O. Brádaigh, "A study on the fatigue life of glass reinforced polymer composites for tidal turbine blades," in *ASME 2011 30th International Conference on Ocean, Offshore and Arctic Engineering*, 2011, pp. 105-112.

[51] (2010). *Det Norske Veritas, DNV-OS-J102, Design and Manufacture of Wind Turbine Blades*. Available: https://rules.dnvgl.com/docs/pdf/DNV/codes/docs/2010-11/DS-J102.pdf

[52] E. K. Gamstedt and B. A. Sjögren, "An experimental investigation of the sequence effect in block amplitude loading of cross-ply composite laminates," *International Journal of Fatigue,* vol. 24, pp. 437-446, 2// 2002.

[53] M. Dawson, P. Davies, P. Harper, and S. Wilkinson, "Effects of conditioning parameters and test environment on composite materials for marine applications," presented at the 2nd IFREMER-ONR: Durability of Composites in a Marine Environment Workshop, Brest, France, 2016.

[54] P. Davies, "Accelerated Aging Tests for Marine Energy Applications," in *Durability of Composites in a Marine Environment*. vol. 208,ed P. Davies and Y. D. S. Rajapakse, New York: Springer, 2014, pp. 165-177.

Appendix 1: Blade element momentum theory (BEMT)

For steady state operation the fluid forces on the blade inside any stream tube must equal the momentum lost from that stream tube:

$$F_A = \left(\frac{2\dot{M}}{N}\right)\left(V_t - U_d(R)\right) \tag{1A.1}$$

where F_A is the sum of the axial components of the lift and drag forces on the blade element inside the tube, N is the number of blades, $\dot{M}$ is the mass flow rate through the tube, U_d is the axial water velocity at the rotor disk, and R is the radius of the disk. Within each stream tube the tangential components of the lift and drag forces sum to give a torque producing force and this imparts angular momentum to the blade. The angular momentum is balanced by an angular momentum of the fluid in the opposite direction, causing wake rotation. With the assumption that the relative resultant water velocities are constant, axial and rotational velocity at the disk can be calculated:

$$U_d = \frac{V_t}{\pi}\sqrt{1 + \gamma^2 + \zeta - \gamma\sqrt{(1 + \gamma^2 - \zeta^2)}} \tag{2A.1}$$

$$V_d = U_d \frac{\sqrt{1+\gamma^2-\zeta^2}-\gamma}{1-\zeta} \tag{3A.1}$$

where V_d is the tangential velocity of the fluid in a stream tube at the rotor disk, ζ is the fraction of axial velocity remaining at the downstream exit of the stream tube, and γ is the local speed ratio given by:

$$\gamma = \frac{\omega_b R}{V_t} \tag{4A.1}$$

where ω_b is the angular velocity of the blade, R is the radius, and V_t is the free stream velocity of the fluid. The blade also has a tangential velocity V_b at the stream tube due to its angular velocity:

$$V_b = \omega_b R \tag{5A.1}$$

The relative velocity at the rotor:

$$V_r = \sqrt{U_d^2 + (V_d + V_b)^2} \tag{6A.1}$$

and the angle between the relative velocity and the plane of the rotor is:

$$\theta = tan^{-1} \frac{U_d}{V_d + V_b} \tag{7A.1}$$

The lift force, *L* (perpendicular) and drag force, *D* (parallel to the fluid velocity), generated by a stream tube on the blade section inside it:

$$L = \frac{1}{2} C_L V_r^2 \rho S \Delta R \tag{8A.1}$$

$$D = \frac{1}{2} C_D V_r^2 \rho S \Delta R \tag{9A.1}$$

where C_L and C_D are the coefficients of lift and drag for the aerofoil selected [33], ρ is the density of the fluid, S is the chord length of the blade at the stream tube radius and ΔR is the radial thickness of the stream tube. The axial and tangential force is:

$$F_A = L \cos\theta + D \sin\theta \tag{10A.1}$$

$$F_C = L \sin\theta + D \cos\theta \tag{11A.1}$$

where F_A is the axial (thrust) force and F_C is the tangential (torque) force acting on the blade by observed stream tube. According to the axial induction factor, maximum power output corresponds to:

$$U_d = \frac{2}{3} V_t \tag{12A.1}$$